JOURNAL OF PROPULSION AND POWER
Vol. 24, No. 6, November–December 2008

Dynamics of Laminar Premixed Flames Forced by Harmonic Velocity Disturbances

Preetham
GE Global Research, Niskayuna, New York 12309
and
H. Santosh and Tim Lieuwen*
Georgia Institute of Technology, Atlanta Georgia 30332-0150

DOI: 10.2514/1.35432

This paper describes the dynamics of constant-burning-velocity premixed flames responding to harmonic velocity disturbances. Results are derived from analytical and computational solutions of the nonlinear *G* equation and compared with available experimental data. It is shown that the flame dynamics are controlled by the superposition of two waves propagating along the flame sheet: those originating at the flame-anchoring point and from flow nonuniformities along the flame. They may either constructively or destructively superpose, and so the overall linear flame response depends upon two Strouhal numbers, St_2 and St_c, related to the amount of time taken for a flow (St_c) and flame-front (St_2) disturbance to propagate the flame length, normalized by the acoustic period. The nonlinear flame response is controlled by flame propagation normal to itself, which smoothens out the wrinkles induced by the forcing at an amplitude-dependent rate. The flame's nonlinear response is shown to exhibit two qualitatively different behaviors. For parameter values at which these disturbances constructively interfere, the nonlinear flame response saturates. When the flame disturbances destructively interfere, the nonlinear transfer function may actually exceed its linear value before saturating. This result explains experimentally observed variations of the nonlinear flame response with frequency.

Nomenclature

$\bar{A}_c, \bar{A}_w$	=	steady-state conical/wedge flame area
A'_c, A'_w	=	fluctuating conical/wedge flame area
c	=	speed of sound
G_c, G_w	=	conical/wedge flame-area velocity transfer function
K	=	convection parameter ($\equiv u_o/u_c$)
k	=	convective wave number ($\equiv \omega_o/u_c$)
L_{avg}	=	time-averaged (nondimensionalized) flame length
L_f	=	steady-state flame length
M_l	=	Markstein length
Q_o	=	steady-state heat release
Q'	=	fluctuating heat release
R	=	burner radius
r	=	radial coordinate
$S_{L,o}$	=	unstretched laminar burning velocity
St	=	Strouhal number ($\equiv \omega_o L_f/u_o$)
St_2	=	reduced Strouhal number [Eq. (27)]
St_c	=	convective Strouhal number [Eq. (29)]
T_b	=	temperature of burned gas
T_u	=	temperature of unburned gas
t	=	nondimensional time
u	=	axial velocity
u_c	=	disturbance propagation velocity
u_o	=	mean axial flow velocity
u'	=	fluctuating axial velocity
v	=	radial velocity
α	=	flame-aspect-ratio parameter [Eq. (22)]
β	=	flame aspect ratio ($\equiv L_f/R$)
ε	=	nondimensionalized fluctuating (axial) velocity amplitude ($\equiv u'/u_o$)
ε_f	=	ε value at flashback
ζ	=	instantaneous flame position (nondimensionalized)
$\zeta_o, \zeta_1, \zeta_2, \zeta_3$	=	functions [Eq. (18)]
η	=	parameter ($\equiv K\alpha$)
ρ_b	=	density of burned gas
ρ_u	=	density of unburned gas
ω_o	=	angular excitation frequency

Received 6 November 2007; revision received 21 April 2008; accepted for publication 15 May 2008.

*Associate Professor, School of Aerospace Engineering. Corresponding Author.

I. Introduction

THIS paper describes an analysis of the linear and nonlinear dynamics of laminar premixed flames responding to harmonic velocity disturbances. The main objective of this work is to predict the heat release response of the flame and to isolate the key nondimensional parameters that characterize these interactions. Although this problem is of great interest from a fundamental standpoint, it is also motivated by pressing practical problems. This paper's focus on premixed flames is motivated by the fact that low-emissions combustion systems usually employ a premixed combustion process. Furthermore, its focus upon harmonically oscillating flow disturbances stems from the fact that these combustion systems are prone to combustion instabilities [1–6] that generally occur when the unsteady combustion process couples with the natural acoustic modes of the combustion chamber, resulting in self-excited oscillations. These oscillations are destructive to hardware and adversely affect performance and emissions. Although the ultimate goal for the modeler is to develop a general theory that describes the dynamics of harmonically perturbed, fully turbulent flames, our focus here upon laminar flames is motivated by the lack of understanding of their dynamics, even in very simple situations.

An unstable combustor's dynamics are controlled by a complex interplay of linear and nonlinear processes. To illustrate, consider an acoustic disturbance with amplitude ε. Referring to Fig. 1, note that this disturbance amplitude stays the same, decreases, or increases depending upon the relative magnitudes of the amplification $H(\varepsilon)$ and damping $D(\varepsilon)$ processes [i.e., whether $H(\varepsilon) = D(\varepsilon)$,

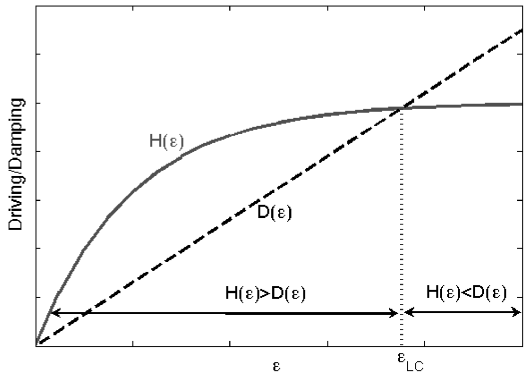

Fig. 1 Qualitative description of the dependence of acoustic amplification $H(\varepsilon)$ and damping $D(\varepsilon)$ processes upon amplitude ε.

$H(\varepsilon) < D(\varepsilon)$, or $H(\varepsilon) > D(\varepsilon)$, respectively]. Linear combustor processes generally control the balance between amplification and damping processes at low amplitudes of oscillation and thus determine the growth rate of inherent disturbances in the combustor. Nonlinear combustor processes control the finite amplitude dynamics of the oscillations. Predicting the limit cycle amplitude of self-excited oscillations requires an understanding of the nonlinear characteristics of $H(\varepsilon)$ and $D(\varepsilon)$. To illustrate, Fig. 1 depicts a situation in which $H(\varepsilon)$ saturates and the two curves cross at the limit cycle amplitude $\varepsilon_{\mathrm{LC}}$.

The focus of this paper is on the heat release dynamics [i.e., to understand the characteristics of $H(\varepsilon)$ in both the linear and nonlinear regime]. This focus on heat release dynamics is motivated by observations that the nonlinear gas-dynamic processes are less significant in many premixed combustors. For example, Dowling [7] suggests that gas-dynamic processes essentially remain in the linear regime, even under limit cycle operation, and that it is the relationship between flow and heat release oscillations that provides the dominant nonlinear dynamics in premixed combustors [i.e., $H(\varepsilon)$]. The primary point of these observations has been confirmed by several experimental studies [8–10], which show that substantial nonlinearities in the heat release response occur at relatively low acoustic amplitudes.

A variety of mechanisms exist for causing nonlinearities in heat release dynamics: for example, local or global flame extinction [7,11], pressure sensitivity of the mass burning rate [12–15], equivalence-ratio oscillations [10,16,17], and flame kinematics [18–21]. It is the latter kinematic mechanism (i.e., the response of the flame-front position as it adjusts to perturbations in flow velocity) that is the focus of this study. Because the flame's position and orientation depends upon the local burning rate and flow characteristics, velocity perturbations cause wrinkling and movement of the flame front. In turn, this modifies its local position as well as its overall area or volume. These velocity disturbances can be acoustic or vortical in nature and thus propagate at the sound speed or with the flow, respectively. To illustrate, Fig. 2 shows data from Shanbhogue et al. [22] of a flame disturbed by vortical-flow oscillations.

Bourehla and Baillot [23], Durox et al. [24], and Baillot et al. [25] performed a systematic experimental and theoretical study of the response of laminar Bunsen flame to velocity perturbations of varying amplitude and frequency. Although their principal observations are similar to those of Blackshear [26], their work appears to be the first systematic characterization of the flame response as a function of perturbation amplitude. Similar to the illustration in Fig. 2, they found that at low frequencies ($f < 200$ Hz) and velocity amplitudes ($u'/u_o < 0.3$), the flame front wrinkles symmetrically about the burner axis due to a convected wave traveling from the burner base to its tip. They also solved the G equation [25] and showed good agreement between predicted and measured flame shapes, even at larger amplitudes of forcing, at which the flame front becomes strongly cusped. The so-called

Fig. 2 Instantaneous image of the flame sheet (solid line) and vorticity isocontours [22].

G equation is a front-tracking equation for the flame position, given by

$$\frac{\partial G}{\partial t} + \mathbf{u} \cdot \nabla G - S_L |\nabla G| = 0 \tag{1}$$

where $G(x, t) = 0$ is an implicit expression defining the instantaneous flame position, $\mathbf{u}$ is the velocity field, and S_L is the laminar burning velocity.

More recent work [22,27,28] has focused on quantifying the *global* heat release response Q' of the flame by, for example, measurements and calculations of the transfer functions $(Q'/Q_o)/(u'_{\mathrm{ref}}/u_o)$ of acoustically forced flames. Significantly, they showed that most of the key flame-response characteristics could be quantitatively predicted by assuming that the flame's heat release was directly proportional to its instantaneous area. The flame area was calculated using the G equation, for which measured velocity fields were used as inputs.

Because of the mutual interaction between the flame position and the flowfield, free boundary problems such as this are difficult to handle analytically. Recent studies [18,27,29–31] have circumvented the analytical difficulties encountered in the fully coupled flame-flow problem by neglecting the coupling of flow perturbations across the flame, as will also be done in this study. The substantially reduced complexity of the approach facilitates a much more transparent analysis; moreover, their results give excellent agreement with experiments in many instances.

In general, however, it should be emphasized that the thermal expansion of gases at the flame front causes the flame to influence the disturbance velocity field upstream of it. As the temperature jump across the flame (T_b/T_u) deviates from unity, there will be an impact upon the approach flow characteristics. It can be shown that the impact of the flame on the acoustic field scales as $(T_b/T_u)^{1/2}$, which is the ratio of the gas impedances across the flame, $\rho_u c_u/\rho_b c_b$. For low-amplitude perturbations, the alteration of the local acoustic field by the flame does not introduce qualitative changes into the flame dynamics, although it may certainly exert quantitative impacts that increase as $(T_b/T_u)^{1/2}$. This assertion has been previously confirmed by Lee and Lieuwen [32], who computationally determined the flame's acoustic near field for various T_b/T_u values, determined the flame-area response, and compared the results with the constant-density analyses of Fleifel et al. [29]. Similarly, it is known [33] that the effect of a stable flame on the vortical approach flow velocity scales approximately as T_b/T_u. As in the acoustic case, there is also a frequency-wave-number dependence, as well as an inverse dependency upon proximity to flame-stability boundaries. As such,

the qualitative linear dynamics of the flame are apparently captured by constant-density analyses for all T_b/T_u values, although the quantitative accuracy of the results deteriorates as T_b/T_u increases. In contrast, the nonlinear dynamics of the flame are only correctly described by such analyses for low T_b/T_u values; that is, new dynamics appear for simultaneously high values of T_b/T_u and perturbation amplitude due to the appearance of a parametric flame instability [34–36].

Previous studies have usually assumed, as we will in this study, that the burning velocity was constant, so that the flame speed is independent of the flowfield (several analyses [37,38] have included mixture-ratio perturbation effects on the flame speed, however). In reality, hydrodynamic strain and flame curvature introduced by the flow oscillations lead to perturbations in flame speed. Because the radius of flame wrinkling is approximately proportional to the inverse of the squared frequency, curvature effects become significant at high frequencies [39]. As shown in Preetham et al. [39], the constant-flame-speed assumption is very accurate at low frequencies, but breaks down when

$$\frac{4\pi^2 M_l(\beta^2+1)^{3/2}L_f f^2}{\beta^4 u_o^2} \sim \mathcal{O}(1)$$

where M_l is the Markstein length, f is the forcing frequency, L_f is the average flame length and β is defined in Eq. (6); for example, this implies that stretch effects become important for $f > 900$ Hz for a methane–air flame with equivalence ratio of 0.7, $M_l \approx 1$ mm, and $u_o = 2$ m/s. A full linear analysis of stretch affected, harmonically forced flames is presented by Preetham et al. [39].

The key contribution of the present work is to provide a systematic treatment of linear and nonlinear flame dynamics in response to harmonically oscillating flow disturbances. The rest of the paper is organized in the following manner: Section II describes the key processes impacting the flame dynamics and the disturbance field. Section III presents the modeling approach and analysis procedure. Section IV presents results that quantify the effects of flame geometry, disturbance field characteristics, and perturbation frequency upon the flames' linear (Sec. IV.A) and nonlinear (Sec. IV.B) characteristics.

II. Basic Considerations

A. Flame Dynamics

Several general comments can be made regarding the flame dynamics that are helpful in understanding the results to be presented later. Basically, velocity perturbations *normal* to the flame are responsible for creating flame wrinkling, and the mean velocity *tangential* to the flame is responsible for convecting these wrinkles along the flame sheet. As noted by Boyer and Quinard [30], the mean velocity tangential to the flame sheet has significant influences on the flame dynamics and significantly alters the flame response with respect to the situation in which the flow is only normal to the flame. These points can be seen from the linearized version of Eq. (1), written in a coordinate system aligned normal to the mean flame position as (see Fig. 3)

$$\frac{\partial \xi}{\partial t} + U_T \frac{\partial \xi}{\partial X} = U'(X,t) \tag{2}$$

where X denotes the coordinate along the mean flame position (assumed to be flat), U_T is the mean velocity component along the X axis, and $\xi(X,t)$ is the perturbed flame position normal to this coordinate. The dynamics of $\partial\xi/\partial X$, which are directly related to that of the flame area itself, is described by the following solution[†]:

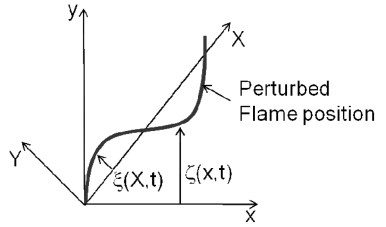

Fig. 3 Coordinate system illustrating the perturbed-flame shape.

$$\frac{\partial \xi(X,t)}{\partial X} = \underbrace{\frac{1}{U_T}\int_0^X \left(\frac{\partial U'(X,t)}{\partial X}\right)_{X\to x',\, t\to\left(t-\frac{X-x'}{U_T}\right)} \mathrm{d}x'}_{\text{flow nonuniformity (particular solution)}} + \underbrace{\frac{1}{U_T}\left(U'\left(X=0, t-\frac{X}{U_T}\right) - U'_{\text{base}}\left(t-\frac{X}{U_T}\right)\right)}_{\text{boundary condition (homogeneous solution)}} \tag{3}$$

As shown, the linear solution to the equation for flame surface area can be decomposed into two canonical components, corresponding to the homogeneous and particular solution of the governing equation. These two canonical solutions have a clear physical significance that can be understood as follows. A spatially uniform velocity disturbance (i.e., one where $\partial U'/\partial X = 0$) only excites the homogeneous solution [second term in Eq. (3)]. This can be understood by first assuming that the flame base moves exactly in step with the particle velocity [i.e., $U'_{\text{base}} = U'(X=0,t)$]. In this case, the entire flame simply moves up and down in a bulk motion without a change in shape or area [32]. However, if a flame-anchoring boundary condition is imposed ($U'_{\text{base}} = 0$), such that the flame remains attached, the flow disturbance excites a flame-front disturbance that originates at the base and propagates along the flame front at a speed of U_T. These homogeneous-solution flame dynamics were extensively analyzed by Fleifel et al. [29]. If the disturbance flowfield is spatially nonuniform (i.e., $\partial U'/\partial X \neq 0$), the particular solution is excited [first term in Eq. (3)]. This results in waves originating at the spatial location(s) of flow nonuniformity that also propagate along the flame.

The flame acts as a low-pass filter to flow disturbances, so that the amplitude of fluctuating flame area associated with those two canonical solutions individually decay with increases in frequency. As such, the transfer function relating the response of the flame area to a spatially uniform velocity disturbance (where only the homogeneous solution is excited), $(A'/\bar{A})/(u'/u_o)$, has a value of unity at zero frequency, decays with frequency, but is generally not identically zero.[‡] In contrast, when the flame is perturbed by a spatially nonuniform disturbance (so that both the homogeneous and particular solution are excited), the flame area consists of a superposition of the two solutions. As such, even though each solution decreases with frequency, their sum has oscillatory behavior and, in cases in which they constructively interfere, can cause the transfer function $(A'/\bar{A})/(u'/u_o)$ to exceed unity. This result was first predicted by Schuller et al. [28] and experimentally observed by Durox et al. [40]. In addition, the two solutions can destructively interfere and, in certain cases, exactly cancel each other so that the resulting transfer function $(A'/\bar{A})/(u'/u_o)$ identically equals zero.

Consider next the basic features of the nonlinear flame dynamics. The key mechanism of nonlinearity is illustrated in Fig. 4. In this illustration, a flame is perturbed by a transient disturbance so that it has a corrugated shape, but is then allowed to relax back to its steady-state planar position through the smoothing action of flame propagation. As such, kinematic processes work to destroy the flame area, as shown by the dashed lines in the bottom sketch [41]. The rate of these area destruction processes depends nonlinearly upon the

[†]In Eq. (3), after evaluating the velocity gradient $\partial U/\partial X$, the integration has to be performed with respect to dx' after replacing the variable X by x' and t by t-$(X$-$x')/U_o$.

[‡]The zero response occurs in two-dimensional flames at frequencies at which the flame-tip motion is zero. In this case, the flame's leading-order area response is also zero.

Fig. 4 Sketch of a flame that is initially wrinkled (top), showing the destruction of the flame area by kinematic restoration processes (bottom).

amplitude and length scale of the flame-front disturbance. Large-amplitude corrugations are smoothed out at a relatively faster rate than small-amplitude perturbations. In the same way, short-length-scale corrugations are smoothed out faster than long length scales of the same disturbance magnitude. As subsequently discussed further, this is the reason that nonlinearity is enhanced at higher disturbance frequencies, which generate shorter-length-scale flame corrugations.

If the disturbance velocity field is spatially uniform (so that only the homogeneous solution is excited), nonlinear effects cause the nonlinear transfer function $(A'/\bar{A})/(u'/u_o)$ to monotonically decrease with disturbance amplitude [21]. Because the scale of flame wrinkling is inversely proportional to frequency (scaling roughly as u_o/f), this nonlinear effect grows with frequency. As such, the flame-area response to a velocity disturbance exhibits saturation characteristics, quite similar to the $H(\varepsilon)$ curve plotted in Fig. 1.

In the general nonlinear case, as in the linear case, the effect of the superposition of the homogeneous and particular solutions upon the overall flame response depends upon whether the two solutions lie in a region of constructive or destructive interference. In particular, if the two solutions lie in a region of destructive interference and are affected unequally by nonlinearity, their superposition may cause the nonlinear transfer function to actually exceed its linear value.

B. Disturbance Field

The velocity field consists of both acoustic and vortical disturbances. Acoustic disturbances propagate with a characteristic velocity equal to the speed of sound. In a uniform flow, vorticity disturbances are convected at the bulk flow velocity u_o. Acoustic properties vary over an acoustic length scale given by $\lambda_a = c/f$, whereas vortical disturbances vary over a convective length scale given by $\lambda_c = u_o/f$. Consequently, in low Mach number flows, these disturbances have substantially different length scales. The vortical mode wavelength is shorter than the acoustic wavelength by a factor equal to the mean flow Mach number: $\lambda_c/\lambda_a = u_o/c = M$.

The characteristics of the instability waves that grow and merge to form large-scale structures are a function of the specific characteristics of the shear layer (such as coflow velocity) and, specifically, of the receptivity of this shear layer to external disturbances. In addition, the phase speed of the convected vortical instability waves are not equal to the flow velocity, but vary with frequency and shear layer characteristics. The instability-wave growth rate similarly varies with frequency and the shear layer characteristics. For example, Michalke's [42] jet flow analysis shows that the phase speed u_c of shear layer instability waves depend upon a Strouhal number based on momentum thickness θ ($S_\theta = f\theta/u_o$) and dimensionless jet radius R/θ. It shows that for all R/θ values, the ratio of u_c/u_o equals unity and 0.5 for low and high Strouhal numbers. For thin boundary layers (e.g., $R/\theta = 100$), the phase velocity actually exceeds the maximum axial flow velocity in a certain S_θ range. This prediction has been experimentally verified [43] and may explain a similar measurement in a Bunsen flame by Ferguson et al. [44]. Furthermore, the variation in convective velocity of the flow disturbance with frequency and geometry has also been observed in perturbed flames. For example, Baillot et al. [20] measured u_c/u_o values of 1.13 and 1.02 at 35 and 70 Hz, respectively, on a conical Bunsen flame. Durox et al. [40] measured $u_c/u_o = 0.5$ values at 150 Hz in an axisymmetric wedge flame.

In general, the disturbance field may have both acoustic and vortical components, for which the relative magnitude depends strongly upon the burner shear layer dynamics [44,45]. The character of the disturbance field can vary significantly between its relative acoustic and vortical components (Birbaud et al. [46]) as well as their spatial structure (such as phase speed); these characteristics will change with experimental configuration, frequency, and amplitude of perturbation. This point is a key motivator for our development of a general theory for arbitrary phase-speed velocity disturbances.

III. Modeling Approach

Figure 5 illustrates the two basic geometries considered. On the left is a conical flame stabilized on a tube, such as a Bunsen flame. On the right is a wedge flame, stabilized on a bluff body. The flames have axial and radial dimensions given by the flame length L_f, and radius R. The instantaneous-flame-sheet location at the radial location r is given by $\zeta(r,t)$.

The analytical approach used here closely follows Baillot et al. [20], Boyer and Quinard [30], and Fleifel et al. [29]. The flame's dynamics are modeled with the front-tracking equation:

$$\frac{\partial \zeta}{\partial t} = u - v\frac{\partial \zeta}{\partial r} - S_L\sqrt{\left(\frac{\partial \zeta}{\partial r}\right)^2 + 1} \tag{4}$$

where u and v denote the axial and radial velocity components, and S_L denotes the flame speed.

The variables t, r, u, and ζ are nondimensionalized by u_o/L_f, R, u_o, and L_f. (Note that the value of L_f and R refer to their nominal values without imposed oscillations.) They are related to the nominal flame speed and average flow velocity by

$$\frac{u_o}{S_L} = \sqrt{\left(\frac{L_f}{R}\right)^2 + 1} \tag{5}$$

The ratio of the flame length to the radius plays an important role in the flame's dynamics and is denoted by β:

$$\beta = \frac{L_f}{R} \tag{6}$$

Given these assumptions, the flame dynamics are given by (from this point on, we use the same symbol for the dimensionless variable):

$$\frac{\partial \zeta}{\partial t} + \sqrt{\frac{1+\beta^2\zeta_r^2}{1+\beta^2}} = u(\zeta,t) - \beta v(\zeta,t)\zeta_r \tag{7}$$

Following previous studies [18,29], we assume that the flame remains anchored at the base; that is,

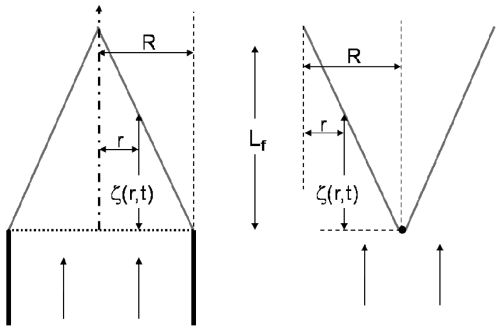

Fig. 5 Illustration of conical (left) and wedge-shaped (right) flame geometries.

$$\zeta(r=1,t)=0 \tag{8}$$

The axial velocity field is specified as

$$u(\zeta,t)=u_o+u'\cos(k\zeta-\omega_o t) \tag{9}$$

Assuming an incompressible disturbance field, appropriate for a vortical- or long-wavelength ($\lambda/L_f \gg 1$) acoustic disturbance, the radial velocity is then

$$v(\zeta,t)=\frac{u'k\tilde{r}}{2}\sin[k\zeta-\omega_o t] \tag{10}$$

where $\tilde{r}=r$ for conical flames and $\tilde{r}=1-r$ for wedge flames.

Here, the wave number k is defined as

$$k=\frac{\omega_o}{u_c}=\left(\frac{\omega_o}{u_o}\right)\left(\frac{u_o}{u_c}\right)=K\left(\frac{\omega_o}{u_o}\right) \tag{11}$$

The two key impacts of the nonuniform flowfield on the flame front, given by the term $\partial u'/\partial X$ in Eq. (3), are captured here by the perturbation amplitude ε and the velocity length scale u_c/ω_o.

The nondimensionalized velocity field is given by

$$u(\zeta,t)=1+\varepsilon\cos[St(K\zeta-t)] \tag{12}$$

$$v(\zeta,t)=\frac{\varepsilon KSt\tilde{r}}{2}\sin[St(K\zeta-t)] \tag{13}$$

where the Strouhal number is

$$St=\frac{\omega_o L_f}{u_o} \tag{14}$$

and the velocity perturbation is

$$\varepsilon=\frac{u'}{u_o} \tag{15}$$

We consider two velocity models for further analytical development. In model A, the velocity is assumed to be purely axial and thus the radial velocity component [Eq. (13)] is neglected. In model B, the two-dimensional velocity field [i.e., both Eqs. (12) and (13)] is considered.

Note that the boundary condition given by Eq. (8) cannot be used for disturbance velocity magnitudes at which the instantaneous flow velocity is lower than the flame speed. In this case, the flame will flash back and Eq. (8) must be replaced by a different condition (e.g., see Dowling [18]). In this study, calculations are performed for velocity magnitudes up to this flashback value ε_f, which is the velocity magnitude at flashback for an axial flow (model A):

$$\varepsilon_f=1-\frac{1}{\sqrt{1+\beta^2}} \tag{16}$$

Two approaches were used to analyze the properties of Eq. (7). Analytical expressions for the linear and nonlinear flame responses were obtained from a perturbation analysis carried out to third order in ε. Terms of $\mathcal{O}(\varepsilon^3)$ are required to determine the leading-order nonlinear correction to the flame transfer function at the forcing frequency. Nonlinear corrections to the average flame length and the flame response at the first harmonic $2\omega_0$ are obtained at $\mathcal{O}(\varepsilon^2)$.

For the fully nonlinear case, Eq. (7) is solved numerically. A robust numerical scheme is necessary that can accurately capture the formation of sharp gradients and cusps in the distorted flame front. Spatial derivatives are discretized using a weighted essentially nonoscillatory scheme developed for Hamilton–Jacobi equations [47]. This scheme is uniformly fifth-order-accurate in regions in which the spatial gradients are smooth and third-order-accurate in discontinuous regions. Derivatives at the boundary nodes are calculated using fifth-order-accurate upwind-differencing schemes so that only the nodes inside the computational domain are used. A third-order-accurate total-variation-diminishing Runge–Kutta scheme [48] is used for time integration. The nondimensionalized spatial and temporal resolution in all the simulations is 10^{-3} and 10^{-4}, respectively. The flame surface area is calculated as a function of time for a given upstream flow velocity perturbation. This is then used to calculate the transfer function relating the flame area at the forcing frequency to the velocity perturbations at the flame base along the centerline.

IV. Results and Discussion

A. Linear Flame Dynamics

In this section, we derive expressions for the flame-area velocity transfer function that generalize the result of Schuller et al. [28] by determining the response of a flame to a disturbance with an arbitrary phase velocity. This transfer function is defined as

$$G=\frac{A'/\bar{A}}{u'_{\mathrm{ref}}/u_o} \tag{17}$$

where u'_{ref} is a reference perturbation velocity.

1. Velocity Model A

a. Flame Shape. The flame position is expanded as [18]

$$\zeta(r,t)=\zeta_o(r)+\zeta_1(r,t)\varepsilon+\zeta_2(r,t)\varepsilon^2+\zeta_3(r,t)\varepsilon^3+\mathcal{O}(\varepsilon^4) \tag{18}$$

The evolution equation for $\zeta_1(r,t)$ is computed here and the $\zeta_2(r,t)$ and $\zeta_3(r,t)$ terms are computed in Sec. IV.B. The mean flame shape in the absence of perturbations is given by

$$\zeta_o(r)=1-r \tag{19}$$

Substituting Eqs. (18) and (19) into Eq. (7), the evolution equation for ζ_1 is

$$\frac{\partial\zeta_1}{\partial t}-\frac{\beta^2}{1+\beta^2}\frac{\partial\zeta_1}{\partial r}-\cos[St\{K(1-r)-t\}]=0 \tag{20}$$

The solution of Eq. (20) given the boundary condition in Eq. (8) is

$$\zeta_1=\zeta_{1,\mathrm{BC}}+\zeta_{1,\mathrm{flow}}=\frac{\sin[(St(r-1+\alpha t))/\alpha]}{(\eta-1)St}-\frac{\sin[St(K(r-1)+t)]}{(\eta-1)St} \tag{21}$$

where

$$\alpha=\frac{\beta^2}{\beta^2+1} \tag{22}$$

$$\eta=K\alpha \tag{23}$$

This equation explicitly decomposes the solution into contributions from boundary conditions and flow-forcing nonuniformities. Note that this expression is valid for both conical and wedge flames. The limit at which $\eta\to 1$ (corresponding to instances in which the two disturbances propagate along the flame at the same speed) is given by

$$\lim_{\eta\to 1}\zeta_1=\frac{(r-1)}{\alpha}\cos\left(St\left\{\frac{(r-1)}{\alpha}+t\right\}\right) \tag{24}$$

B. Flame-Area Velocity Transfer Function: Relative Contribution of Different Sources. The surface area for a conical flame is given by

$$\frac{A_c(t)}{\bar{A}_c}=2\frac{\int_0^1 r\sqrt{1+\beta^2(\partial\zeta/\partial r)^2}\,\mathrm{d}r}{\sqrt{1+\beta^2}} \tag{25}$$

Using Eqs. (18), (19), and (21) in Eq. (25) and defining

$$G_c = \frac{A_c'/\bar{A}_c}{u'(y=0)/u_o}$$

[i.e., $u'_{\text{ref}} = u'(y=0)$] yields

$$G_c(St_2,\eta) = G_{c,\text{BC}} + G_{c,\text{flow}} = 2\left(\frac{e^{iSt_2} - 1 - iSt_2}{(\eta-1)St_2^2}\right) + 2\left(\frac{1 - e^{i\eta St_2} + i\eta St_2}{\eta(\eta-1)St_2^2}\right) = 2\left(\frac{\eta(1-e^{iSt_2}) + e^{i\eta St_2} - 1}{\eta(1-\eta)St_2^2}\right) \tag{26}$$

where

$$St_2 = \frac{St}{\alpha} = \frac{St(1+\beta^2)}{\beta^2} \tag{27}$$

Following a similar procedure, the following result can be obtained for wedge flames:

$$G_w(St_2,\eta) = G_{w,\text{BC}} + G_{w,\text{flow}} = 2\left(\frac{1 + i(i+St_2)e^{iSt_2}}{(\eta-1)St_2^2}\right) + 2\left(\frac{(1-i\eta St_2)e^{i\eta St_2} - 1}{\eta(\eta-1)St_2^2}\right) = 2\left(\frac{\eta - 1 + i(i+St_2)\eta e^{iSt_2}) + (1-i\eta St_2)e^{i\eta St_2}}{\eta(\eta-1)St_2^2}\right) \tag{28}$$

Equations (26) and (28) reduce to the expressions previously developed by Schuller et al. [28] when the phase speed of the disturbances is equal to that of the mean flow (i.e., $K = 1$) (note that they refer to St_2 as ω^* and α as $\cos^2\alpha$). Thus, the linear flame transfer functions for both the conical and wedge flames [Eqs. (26) and (28)] depend upon two parameters: St_2 and η. It is useful to define a new Strouhal number based upon the convective velocity u_c of the flow disturbances St_c, which naturally arises in the two transfer functions [Eqs. (26) and (28)] and equals ηSt_2:

$$\eta St_2 = KSt = \left(\frac{u_o}{u_c}\right)\left(\frac{\omega_o L_f}{u_o}\right) = \frac{\omega_o L_f}{u_c} = St_c \tag{29}$$

These two Strouhal numbers are related to the amount of time taken for a flow (St_c) and flame-front (St_2) disturbance (which is ultimately created by a flow disturbance) to propagate the flame length, normalized by the acoustic period.

Before looking at the total flame transfer function, it is useful to understand the relative contribution from the boundary-condition and flow-forcing nonuniformities. Their ratio is given by

$$\frac{G_{c,\text{flow}}}{G_{c,\text{BC}}} = \frac{1 - e^{i\eta St_2} + i\eta St_2}{\eta(e^{iSt_2} - 1 - iSt_2)} \tag{30}$$

$$\frac{G_{w,\text{flow}}}{G_{w,\text{BC}}} = \frac{(1-i\eta St_2)e^{i\eta St_2} - 1}{\eta(1-(1-iSt_2)e^{iSt_2})} \tag{31}$$

The magnitude of this ratio is identical for both wedge and conical flames (see Fig. 6). The phase of this ratio is different for conical (not shown here) and wedge flames (plotted in Fig. 7).

It is instructive to analyze the characteristics of this ratio for limiting values of the parameters η and St_2. First, note that in the $\eta \to 0$ limit (i.e., a spatially uniform disturbance), the flame dynamics for both the wedge and conical flames are controlled exclusively by the boundary-condition term, irrespective of the Strouhal number:

$$\lim_{\eta\to 0}\left(\frac{G_{c,\text{flow}}}{G_{c,\text{BC}}}\right) = \lim_{\eta\to 0}\left(\frac{G_{w,\text{flow}}}{G_{w,\text{BC}}}\right) = 0 \tag{32}$$

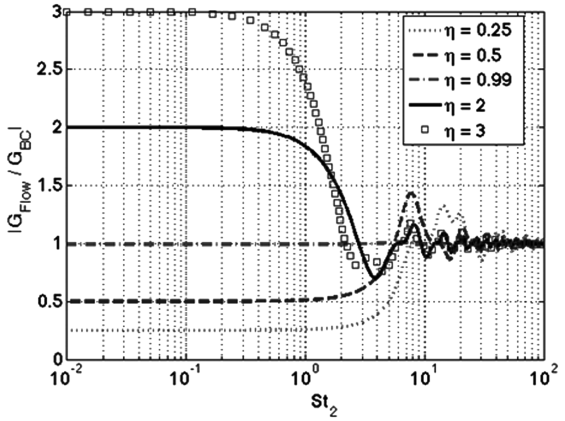

Fig. 6 Strouhal number dependence of the magnitude of the ratio of the transfer functions due to the flow-nonuniformity and boundary-condition terms for different values of η.

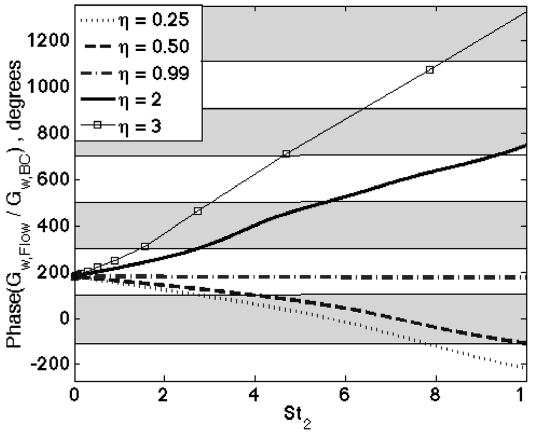

Fig. 7 Strouhal number dependence of the phase of the ratio of the transfer functions due to the flow-forcing and boundary-condition terms for wedge flames. Shaded regions indicate points at which boundary-condition and flow-nonuniformity terms are in phase.

This result reflects the fact that only the homogeneous solution is excited when the flow disturbance is uniform.

In the $St_2 \to 0$ limit, the relative contribution of the two terms is determined by the value of the parameter η:

$$\lim_{St_2\to 0}\left(\frac{G_{c,\text{flow}}}{G_{c,\text{BC}}}\right) = \left(\frac{G_{w,\text{flow}}}{G_{w,\text{BC}}}\right) = -\eta \tag{33}$$

The boundary-condition and flow-forcing terms dominate when $\eta < 1$ and $\eta > 1$, respectively. For long flames ($\beta \gg 1$), this physically corresponds to situations in which the disturbance-phase velocity is greater than and less than the mean flow velocity, respectively. The two terms tend toward equal magnitudes when $\eta = 1$,[§] as shown in Fig. 6. Note also that the flow disturbance and boundary-condition terms are 180 deg out of phase for low St_2 values (see Fig. 7). In the intermediate Strouhal number range (say, $1 < St_2 < 10$), either the flow forcing or the boundary condition may dominate, depending upon η and St_2.

In the limit of $St_2 \gg 1$, the contribution from both the boundary conditions and flow-forcing term are equal, as shown in Fig. 6:

[§]Some care is required in analyzing this $\eta = 1$ result, because the two terms tend to have equal magnitudes and are 180 deg out of phase. The overall response is not zero, however, because the common denominator $\eta = 1$ in Eqs. (26) and (29), which has been canceled out when taking their ratio, causes their sum to have a nonzero value.

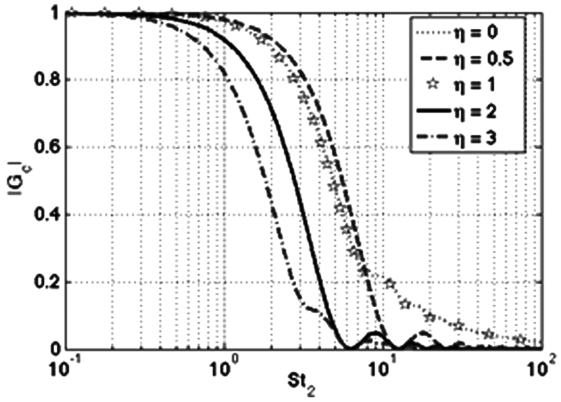

Fig. 8 Axisymmetric conical linear transfer-function $G_c(St_2, \eta)$ magnitude dependence upon the reduced Strouhal number St_2 for different values of η.

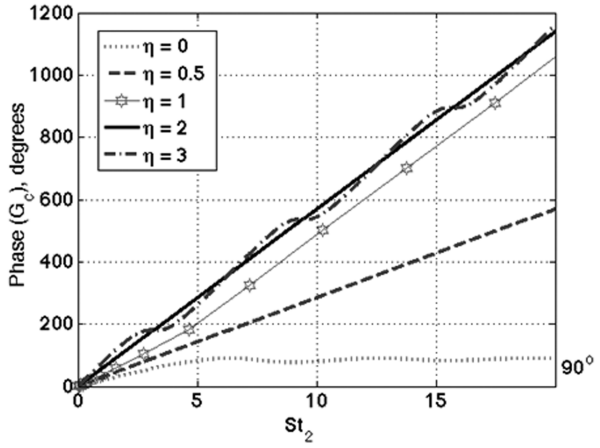

Fig. 9 Axisymmetric conical linear transfer-function $G_c(St_2, \eta)$ phase dependence upon the reduced Strouhal number St_2 for different values of η.

$$\lim_{St_2 \to \infty} \left(\frac{G_{c,\text{flow}}}{G_{c,\text{BC}}} \right) = -1 \qquad \lim_{St_2 \to \infty} \left(\frac{G_{w,\text{flow}}}{G_{w,\text{BC}}} \right) = -e^{i(\eta-1)St_2} \tag{34}$$

Equation (34) also shows that in this limit, the relative magnitude contribution of these two terms is independent of η (assuming that the ηSt_2 product does not simultaneously go to zero). Furthermore, in the limit of $St_2 \gg 1$, the two terms are always out of phase for conical flames, irrespective of the Strouhal number and η. In contrast, for wedge flames, the phase difference between the two contributions monotonically increases with St_2, as shown in Fig. 7 (the shaded bands in the figure indicate regions of constructive interference).

c. Flame-Area Velocity Transfer Function: Overall Features. The dependence of the magnitude and phase of the total conical-flame transfer function $G_c(St_2, \eta)$ upon St_2 at several η values is plotted in Figs. 8 and 9, respectively. Consider the magnitude results first. As previously noted by Schuller et al. [28], the transfer-function gain is identical in the cases in which $\eta = 0$ or 1. Physically, this corresponds to cases in which the disturbance velocity is uniform, $\eta = 0$, or its phase speed matches the flame-front disturbance velocity, $\eta = 1$. The gain transfer function differs for all other disturbance-phase velocity cases. Note also that the gain value is always less than one and generally decreases monotonically with St_2, although there is some ripple at higher St_2 values due to constructive and destructive interference between $G_{c,\text{flow}}$ and $G_{c,\text{BC}}$. The transfer-function phase starts at 0 deg at low St_2 and initially increases monotonically with St_2. For the $\eta = 0$ case, the phase tends to a limiting value of 90 deg for large St_2 (see Fig. 9). In all other cases, the phase monotonically increases, and for high values of η and St_2, the phase curves collapse into a single line.

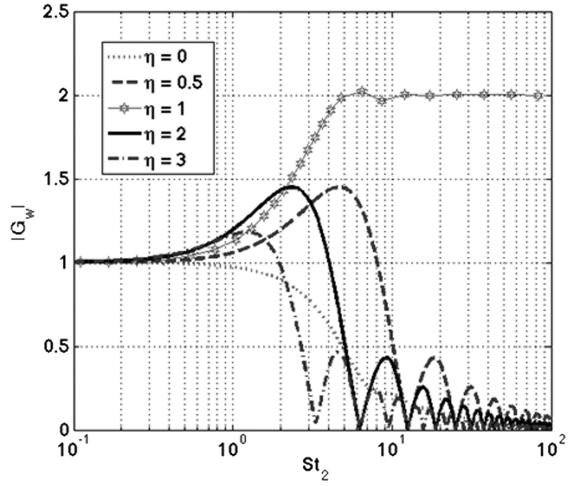

Fig. 10 Axisymmetric wedge linear transfer-function $G_w(St_2, \eta)$ amplitude dependence upon the reduced Strouhal number St_2 for different values of η.

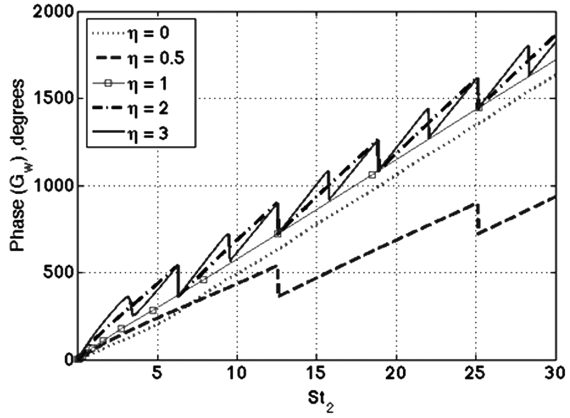

Fig. 11 Axisymmetric wedge linear transfer-function $G_w(St_2, \eta)$ phase dependence upon the reduced Strouhal number St_2 for different values of η.

For wedge flames, the gain and phase of the flame transfer function $G_w(St_2, \eta)$ are shown in Figs. 10 and 11 respectively. Note that, similar to conical flames, all gain values tend toward unity at low St_2. However, only in the uniform velocity case, $\eta = 0$, does the gain then decrease with increases in St_2, as might be expected. In all other cases, the gain increases to values of greater than unity, due to the constructive superposition of $G_{w,\text{flow}}$ and $G_{w,\text{BC}}$. This amplification of the flame response over its quasi-steady value was previously predicted by Schuller et al. [28] and confirmed in measurements by Durox et al. [40]. The magnitude and St_2 value of the peak value of this amplification region is controlled by η. As shown in Fig. 10, the magnitude of the peak value of G_w initially increases from unity as η increases with zero, reaches a maximum at $\eta = 1$, and then decreases back to unity with further η increases. Next, note from Fig. 11 that the phase increases with St_2, with similar characteristics for all η values. To summarize, η and St_2 play a significant role in determining the effect of superposition between flow disturbance nonuniformity and boundary-condition terms. This point is critical to understanding the effect of these parameters on the nonlinear flame dynamics, discussed in Sec. IV.B.

2. *Velocity Model B*

In this section, we present the analysis for the flame-area transfer function based on the velocity field specified in model B, which has an additional radial velocity component. Following the same approach as in Sec. IV.A.1, the conical-flame-area transfer function can be expressed as

$$G_c = 4i\left(\frac{\eta(1-e^{iSt_2})+e^{i\eta St_2}-1}{\eta(1-\eta)(2i+\beta\eta St_2)St_2^2}\right)+2\beta\left(\frac{i(2\eta-1)e^{i\eta St_2}+\eta^2(-i+(\eta-1)St_2)e^{iSt_2}-(\eta-1)^2(-i+\eta St_2)}{\eta(\eta-1)^2(2i+\beta\eta St_2)St_2^2}\right) \tag{35}$$

where the reference velocity for the transfer function is based upon the normal velocity at the flame base, $u'_{\text{ref}} = u'_n(y=0)\sqrt{1+\beta^2}$. To compare with model A, the normal velocity is also scaled by $\sqrt{1+\beta^2}$ so that the axial flow velocity in the two models is the same at $St = 0$ [alternatively, u'_{ref} for model A could be defined as $u'_n(y=0)$]. Similar to Eq. (26), G_c can be expressed as contributions from boundary conditions and flow nonuniformity, as has been shown in the first author's thesis [49].

The transfer-function gains based on models A and B are compared in Fig. 12. It can be seen that the results are identical for $\eta = 0$, but differ for other η values. However, these differences are not substantive: note the similar qualitative behavior of the cases for models A and B for all η values. Similarly, the phase predictions are very similar for both velocity models (see Fig. 13).

The perturbation velocity magnitude for model B varies along the flame, in contrast to model A. In this case, some care is required in defining a physically useful reference velocity u'_{ref} for the transfer function (see also the discussion by Lee and Lieuwen [32]). For example, if the perturbation velocity magnitude is near zero at the base of the flame, but has much larger values everywhere else, then defining the transfer function based upon the perturbation velocity at the flame base will lead to physically misleading results. In the same way, if only the axial velocity were used in the transfer function in Eq. (35), G_c would initially grow with St_2 because of the corresponding increase in radial velocity [see Eq. (13)]. Such behavior does not reflect any new physical phenomenon, but is only an artifact of the choice in normalization velocity. Similarly, the appropriate definition of reference velocity is different for conical and wedge flames, because of the significantly different spatial distribution in flame area. This point emphasizes the need for careful consideration of reference velocity when comparing flame transfer functions across different perturbation velocity fields or geometries.

The close similarities between the results of models A and B provide a very helpful insight for modeling flame dynamics. Specifically, they show that a detailed spatial characterization of the perturbation velocity field is not needed to obtain a reasonable description of the flame response (assuming that appropriate normalization velocities for the transfer function are used for comparisons, as already detailed). This result can be understood from Eq. (3), which shows that the flame-area dynamics are controlled by 1) the perturbation velocity normal to the flame and 2) the spatial scale over which the perturbation velocity varies. As long as the two disturbance velocity fields are similar in these two respects, this discussion shows that the resulting flame-area response is also similar. This is a helpful result for the present study, for which the goal is not to simulate the exact disturbance field of any particular experimental setup, but rather to elucidate the key physical processes and nondimensional parameters that influence the flame's dynamics. This shows that such insight can be gained from simplified representations of the velocity field, as long as they retain the two critical components already noted.

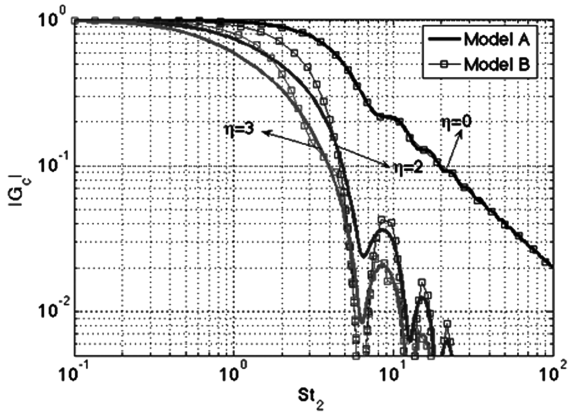

Fig. 12 Axisymmetric conical linear transfer-function G_c amplitude dependence upon the reduced Strouhal number St_2 for different values of η; $\beta = 1$.

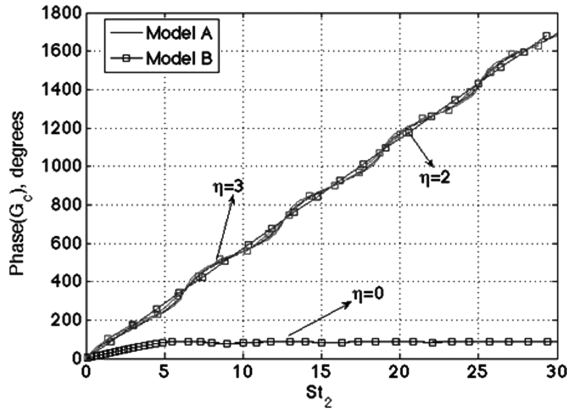

Fig. 13 Axisymmetric conical linear transfer-function G_c phase dependence upon the reduced Strouhal number St_2 for different values of η; $\beta = 1$.

B. Nonlinear Flame Dynamics

We turn our attention next to the nonlinear flame response. Before considering specific results in the nonlinear case, several general conclusions can be drawn from analysis of the governing equation. Note that nonlinearities in the flame-area response arise from three sources. The first is the nonlinear flame dynamics, through the term $\sqrt{1+\beta^2(\partial\zeta/\partial r)^2}$ in Eq. (7). The second is the static nonlinearity introduced through the dependence of the flame area upon the flame position gradient through a term with the same form, $\sqrt{1+\beta^2(\partial\zeta/\partial r)^2}$ [see Eq. (25)]. In both of these cases, the nonlinearity is purely geometric in origin and is introduced by the relationship between the instantaneous-flame-front normal and flame position gradient. The third nonlinearity is due to the flow forcing itself and is due to the dependence of the disturbance velocity at the flame front upon the flame position, $u(\zeta, t)$.

The fact that the first two sources of nonlinearity are identical can be used to write the final expressions for the flame area in a revealing form. By substituting Eq. (7) in the expressions for flame area, the term

$$\sqrt{\frac{1+\beta^2(\partial\zeta/\partial r)^2}{1+\beta^2}}$$

which appears in both of the area integrals, can be written as

$$\sqrt{\frac{1+\beta^2(\partial\zeta/\partial r)^2}{1+\beta^2}} = u(\zeta,t) - \frac{\partial\zeta}{\partial t} \tag{36}$$

Thus, *the explicit form of the nonlinearity disappears*. Nonlinearities in flame-front dynamics are included in the $\partial\zeta/\partial t$ term and those due to flow-forcing nonlinearities are included in the $u(\zeta, t)$ term. Based upon Eq. (36), the following observations can be made regarding the effects of various parameters upon nonlinearity in the flame's response to flow perturbations.

Strouhal number: At low Strouhal numbers St, the unsteady term in Eq. (36) is negligible. Moreover, the ζ dependence of the velocity

field, $u(\zeta, t)$, is weak, at least for the velocity fields considered here. Thus, the flame area's velocity response remains linear for low Strouhal numbers, because St is the dimensionless ratio of the flame-response time to the perturbation period. This point shows that the flame's *nonlinear area response is an intrinsically dynamic phenomenon; its quasi-steady response is linear*.

Flow uniformity: Nonlinearities in the $u(\zeta, t)$ term are directly due to nonuniformity in flow disturbances. Thus, the contribution of this term to flame-area nonlinearities is suppressed in the $\eta \to 0$ limit.

Boundary conditions: If the flame remains anchored at the attachment point, as it is in this study, then $\partial\zeta/\partial t$ is identically zero at this point. As such, the flame-area perturbations in the vicinity of the attachment point exhibit a linear dependence upon velocity amplitude. Nonlinearities grow monotonically in magnitude with downstream distance from the attachment point. As such, the axisymmetric conical flame exhibits a more linear response than the axisymmetric wedge flame for comparable values of ε, because most and very little, respectively, of the flame area is concentrated near the attachment point, where the flame dynamics are linear. This discussion also shows the potential coupling between the flame kinematic and flame-holding sources of nonlinearity.

Flame aspect ratio: β is an important nonlinearity parameter for this problem because the flame dynamics become linear when $\beta \gg 1$ (i.e., when the flame is very long). This can be seen by noting that the left side of Eq. (7) becomes linear in this case:

$$\sqrt{1+\beta^2(\partial\zeta/\partial r)^2} = \pm\beta\partial\zeta/\partial r$$

In this case, the flame dynamics are linear, although the flow-forcing term need not be.

As discussed in Sec. IV.A.2 in the context of linear flame dynamics, different velocity fields with similar spatial scales of variation and surface-area-weighted normal velocities will give similar flame responses. This point also carries over to the nonlinear flame dynamics, as illustrated in Fig. 14, which plots the dependence of the flame-area response upon perturbation velocity amplitude for models A and B, showing that the results are almost identical.

Next, we derive an expression for the lowest-order nonlinear correction to the flame-area velocity transfer function using model A. Returning to the perturbation expansion for the flame position in Eq. (18), the following equations describe the dynamics of the second- and third-order correction terms ζ_2 and ζ_3:

$$\frac{\partial\zeta_2}{\partial t} - \alpha\frac{\partial\zeta_2}{\partial r} + \frac{\alpha(1-\alpha)}{2}\left(\frac{\partial\zeta_2}{\partial r}\right)^2 + \zeta_1 KSt\sin[St\{K(1-r)-t\}] = 0$$

$$\frac{\partial\zeta_3}{\partial t} - \alpha\frac{\partial\zeta_3}{\partial r} + \frac{\alpha^2(1-\alpha)}{2}\left(\frac{\partial\zeta_1}{\partial r}\right)^3 + \alpha(1-\alpha)\left(\frac{\partial\zeta_1}{\partial r}\right)\left(\frac{\partial\zeta_2}{\partial r}\right) + \frac{\zeta_1^2K^2St^2}{2}\cos[St\{K(1-r)-t\}] + \zeta_2 KSt\sin[St\{K(1-r)-t\}] = 0 \tag{37}$$

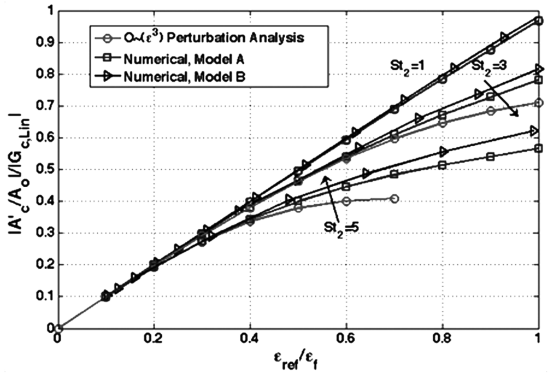

Fig. 14 Dependence of flame-area fluctuations upon disturbance velocity amplitude for axisymmetric conical flames at $\eta = 1$, where $\varepsilon_{\mathrm{ref}} = u'_{\mathrm{ref}}/u_o$.

The solution of Eq. (37), subject to the boundary condition in Eq. (8), is given in the first authors's thesis [49]. In the ensuing discussion, we focus upon the total heat release response. Defining the flame-area velocity transfer function at the fundamental frequency as

$$G_{\omega_o} = \frac{A'(\omega_o)/\bar{A}_o}{u'(\omega_o)/u_o}$$

yields

$$G_{\omega_o} = G_{\mathrm{lin}} + \varepsilon^2\left(\frac{\tilde{A}_{\omega_o}e^{iK\alpha St_2}}{8K\alpha^3(K\alpha-1)^5St_2^2} + \frac{\tilde{B}_{\omega_o}e^{iSt_2}}{8\alpha^2(K\alpha-1)^5St_2^2} + \frac{\tilde{C}_{\omega_o}K(\alpha-1)e^{i(2-K\alpha)St_2}}{8(K\alpha-2)^3(K\alpha-1)^5St_2^2} + \frac{\tilde{D}_{\omega_o}K^2e^{i(2K\alpha-1)St_2}}{8(2K\alpha-1)^2(K\alpha-1)^5St_2^2} + \frac{\tilde{E}_{\omega_o}}{2K\alpha^3(K\alpha-2)^3(2K\alpha-1)^2St_2^2}\right) \tag{38}$$

where G_{lin} refers to the linear transfer function [Eq. (26)]. Expressions for the coefficients $\tilde{A}_{\omega o}$–$\tilde{E}_{\omega o}$ are contained in first author's thesis [49].

The conical transfer functions evaluated using the analytical result [Eq. (38)] are compared with numerical simulations for a representative case in Fig. 14. Although not shown, comparable results are obtained for wedge flames using Eq. (38). Nonlinearity is enhanced as the velocity amplitude or the Strouhal number increases. As expected, the perturbation analysis is accurate at higher-velocity amplitudes when the Strouhal number is low.

The linear component of the transfer function in Eq. (38) is described by only two parameters [i.e., $G_{\mathrm{lin}} = G(St_2, \eta)$]. For the general nonlinear case, the gain G is also a function of ε and β [i.e., $G = G(St, K, \varepsilon, \beta)$]. Also, as can be seen from the contribution of the nonlinear terms to the transfer function in Eqs. (38), two new characteristic timescales arise that are represented by the nondimensional terms $(2\text{-}K\alpha)St_2 = 2St_2\text{-}St_c$ and $(2K\alpha\text{-}1)St_2 = 2St_c\text{-}St_2$. The boundary-condition and flow-nonuniformity terms give rise to the characteristic times represented by the terms containing St_2 and St_c, respectively [the terms with the coefficients $\tilde{B}_{\omega_o}$ and $\tilde{A}_{\omega_o}$ in Eq. (38)]. In addition, the timescales represented by the terms $(2K\alpha\text{-}1)St_2$ and $(2\text{-}K\alpha)St_2$ arise as a result of the nonlinear interaction between these two sources of flame disturbance. Hence, to the order of approximation considered here, the nonlinear characteristics of the flame dynamics are controlled by the superposition of the flame disturbances represented by the terms St_2, St_c, $2St_2\text{-}St_c$, and $2St_c\text{-}St_2$. As anticipated earlier, the nonlinear flame dynamics is qualitatively different, depending upon whether the flame disturbances have a single- or multiple-characteristic timescale. The ensuing discussion will consider the former case first and the multiple-timescale case next.

Consider the two limiting cases $\eta = 0$ and $\eta = 1$, wherein all the preceding discussed timescales reduce to a single one, represented by the term St_2. The flame dynamics in the uniform-velocity case ($\eta = 0$) are exclusively controlled by the boundary condition. In this case, the transfer-function expressions reduce to

$$\lim_{\eta\to 0} G_{c,\omega_o} = \frac{2(1-e^{iSt_2}+iSt_2)}{St_2^2} - \varepsilon^2(1-\alpha) \times\left(\frac{6\alpha+iSt_2+2i\alpha St_2+e^{iSt_2}(-6\alpha-iSt_2+4i\alpha St_2+(\alpha-1)St_2^2)}{4St_2^2\alpha^2}\right) \tag{39}$$

$$\lim_{\eta\to 0} G_{w,\omega_o} = \frac{2(-1+e^{iSt_2}(1-iSt_2))}{St_2^2} - \varepsilon^2(1-\alpha) \times\left(\frac{6\alpha(-1+e^{iSt_2}-iSt_2e^{iSt_2})-3\alpha St_2^2e^{iSt_2}+i(\alpha-1)St_2^3e^{iSt_2}}{4St_2^2\alpha^2}\right) \tag{40}$$

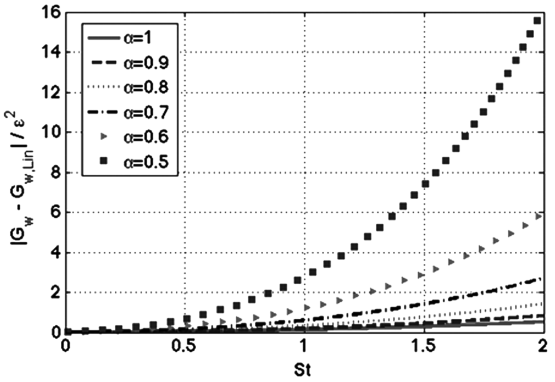

Fig. 15 Dependence of nonlinear part of the transfer function for axisymmetric wedge flames at $\eta = 1$.

Note that in the limit of long flames ($\beta \gg 1 \Rightarrow \alpha \to 1$), the nonlinear contribution to the transfer function disappears for both conical and wedge flames.

Figure 15 shows the variation of the nonlinear part of the transfer function for wedge flames as a function of the Strouhal number when $\eta = 1$ for different values of α. As expected, for low Strouhal numbers ($St \to 0$), the contribution from the nonlinearities goes to zero. This is due to the absence of any destructive interference effect leading to a monotonic increase in the nonlinear contribution with increasing Strouhal number. Moreover, the contribution to the gain is substantially enhanced as the flame gets shorter (i.e., lower values of α), consistent with the flame-aspect-ratio argument in the introduction of this section.

Hence, the presence of a single-characteristic timescale for the $\eta = 0$ and $\eta = 1$ cases causes the nonlinear contribution to monotonically increase with increasing Strouhal number and/or decreasing flame aspect ratio. As subsequently discussed further, *it is only for these two cases that the nonlinearities always lead to a reduction in the magnitude of the total transfer function*. These conclusions are valid even at higher-velocity amplitudes, as shown by numerical simulations in Figs. 16–18, which plot the St_2 dependence of the gain and phase of the nonlinear transfer function upon St_2. Results are shown for two convective wave speeds, $\eta = 0$ and $\eta = 1$, allowing for a comparison of the effects of nonlinearities from boundary conditions alone and the combined effect of boundary conditions and flow disturbance nonuniformity. Consider the gain curves first (Figs. 16 and 18). As predicted earlier, the response tends to its linear value in all cases at low St_2. In the $\eta = 0$ case, nonlinear effects are more apparent at high St_2. For the wedge flame in Fig. 18, the response is considerably nonlinear even at moderate values of Strouhal number. The enhanced nonlinear response of wedge over cone flames is explained by the boundary-conditions argument discussed earlier.

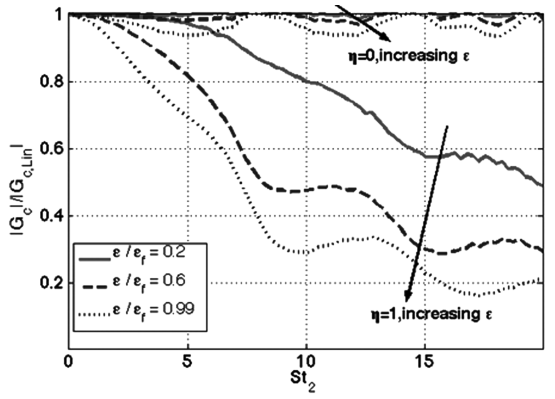

Fig. 16 Strouhal number dependence of the ratio of the magnitude of the flame-area velocity transfer function to its linear value for the axisymmetric conical flame; $\beta = 2$.

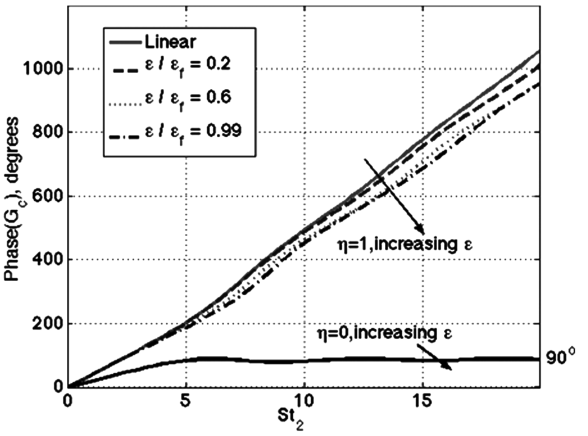

Fig. 17 Strouhal number dependence of the phase of the flame-area velocity transfer function for the axisymmetric conical flame; $\beta = 2$.

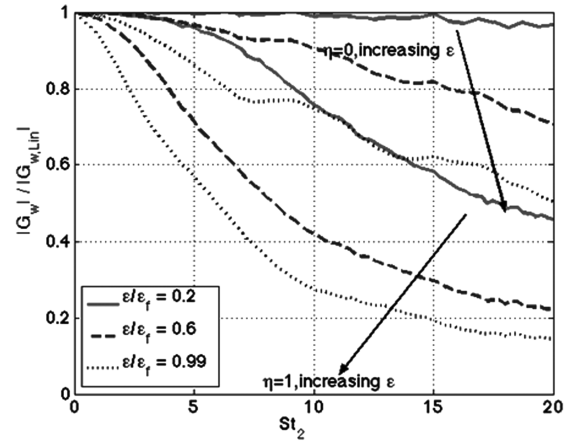

Fig. 18 Strouhal number dependence of the ratio of the magnitude of the flame-area velocity transfer function to its linear value for the axisymmetric wedge flame; $\beta = 2$.

Turning to the $\eta = 1$ case, note the substantial reduction in flame area relative to its linear value; that is, there is a substantial degree of gain saturation. Although plotted in a different form, the resulting gain curves look quite similar to the qualitative plot of $H(\varepsilon)$ in Fig. 1. In agreement with the Strouhal number argument discussed earlier, the degree of nonlinearity increases with St_2. As shown in Figs. 16 and 18, the gain for the conical and wedge flames decreases by about 80 and 85%, respectively, (at $\varepsilon = \varepsilon_f$ in the $St_2 = 20$ and $\eta = 1$ case). In contrast, the gain never drops below 5% of its linear value for conical flames and 55% of its linear value for wedge flames in the $\eta = 0$ case. Moreover, unlike the $\eta = 0$ case, the phase of the area response for both the conical (see Fig. 17) and wedge flames (not shown here) exhibits a strong amplitude dependence. These results indicate the extent to which flow nonuniformities can significantly modify the nonlinear flame response.

We next consider the case in which $\eta \neq 0$ or 1 and the flame dynamics are controlled by the superposition of flame disturbances with the four different characteristic timescales discussed earlier. In contrast to the preceding results, interactions between the boundary-condition and flow-forcing nonuniformity solutions cause a nonmonotonic variation in the transfer-function gain with disturbance amplitude. To illustrate, Fig. 19 shows the flame response for a wedge flame when $\eta = 2$ (i.e., $\alpha = 0.8$ and disturbances are traveling at $0.4u_o$). Note that the gain results are not normalized by their linear value here. The gain result indicates that in the $5 < St_2 < 8$ range, the nonlinear transfer function actually *exceeds* its linear value. This result can be understood by noting that this behavior occurs in the vicinity of the regions in which the linear transfer function achieves a minimum. At these St_2 values, the

contributions from the boundary conditions and the flow-forcing terms destructively interfere, leading to low linear gains. As the velocity amplitude is increased, nonlinearities cause the gain due to both the boundary conditions and the flow-forcing terms to decrease. However, because the relative ages of the two disturbances are unequal, the discussion in the context of Fig. 4 shows that the magnitude of their gain reductions is different. Because the individual gain decreases by different amounts, the total gain does not go to zero at the St_2 value at which the linear gain is zero, but actually shifts to a higher St_2 value in the $\varepsilon = 0.2\varepsilon_f$ case. At higher disturbance levels, the two terms never exactly cancel and the gain does not go to zero. Rather, there is a monotonic decrease in the gain of the transfer function with an increase in velocity amplitude. Analogous behavior also occurs in conical flames, although less significantly.

These predictions compare well to related measurements of Durox et al. [40] on wedge flames, where the phase speed of the disturbances was half the mean flow speed. They obtained measurements at four forcing amplitudes $\varepsilon \sim 0.05$–0.2 and $\beta \sim 5.6$. Interestingly, they found both increases and decreases in the transfer-function gain with changes in disturbance amplitude, depending upon the Strouhal number. Their results are reproduced in Fig. 20. The transfer functions plotted here equal the ratio of the fluctuating CH^* emission intensity to the velocity disturbance amplitude slightly above the burner exit. Note the strong similarities between their measurement and the predictions from Fig. 19. In the $2 < St_2 < 5$ regions in which the transfer function exceeds unity, the nonlinear gain monotonically decreases with disturbance amplitude. In the $5 < St_2 < 8$ range, the nonlinear transfer function first increases with disturbance amplitude, then decreases.

Using the perturbation analysis, the nonlinear contribution to the wedge-flame transfer function is shown for varying phase speeds at a unity Strouhal number in Fig. 21. It shows that the nonlinear contribution increases with K (i.e., when the phase speed of the disturbances is less than the mean flow speed). This is a direct manifestation of the flow-uniformity argument discussed earlier. As noted earlier, nonlinearity decreases with increase in the flame aspect ratio (i.e., increasing α), consistent with the flame-aspect-ratio argument. Note that this result is valid for a low Strouhal number case wherein the linear gain does not go to zero for both the conical and wedge flames. Hence, the gain monotonically decreases with increasing disturbance amplitude. However, for higher Strouhal numbers, the linear gain goes to zero at certain η values. It is only in the vicinity of these η values that we find the corresponding increase in nonlinear flame transfer function. This result prominently highlights the sensitivity of the flame response to the phase speed of the disturbances. Moreover, it demonstrates how the competition between boundary-condition and flow-nonuniformity terms can significantly impact the flame-response behavior.

These results have important implications upon the type of bifurcations that may be observed in unstable combustors. In situations in which the amplification and damping curves resemble that qualitatively shown in Fig. 1, only supercritical bifurcations will occur and a single stable limit cycle amplitude ε_{LC} is possible. In situations in which the gain exceeds, then is less than, the linear gain (see Fig. 19) (that is, it exhibits an inflection point), multiple stable solutions for the instability amplitude may exist, and subcritical bifurcations are possible. This can be seen from Fig. 22, which plots the dependence of $A'_w/\bar{A}_w$ vs ε for $St_2 = 6.25$, $K = 2.5$, and $\alpha = 0.8$. This curve represents $H(\varepsilon)$.

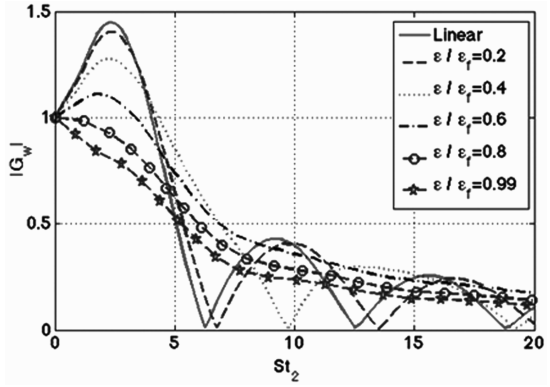

Fig. 19 Strouhal number dependence of the magnitude of the flame-area velocity transfer function for the axisymmetric wedge flame; $\beta = 2$ and $\eta = 2$.

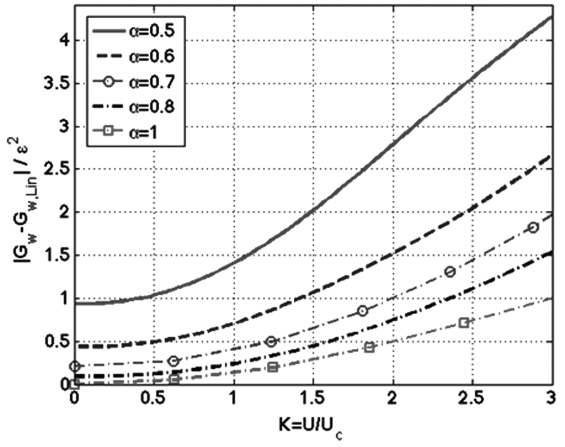

Fig. 21 Dependence of nonlinear part of the transfer function on the phase speed of the disturbances (K) for axisymmetric wedge flames; $St = 1$.

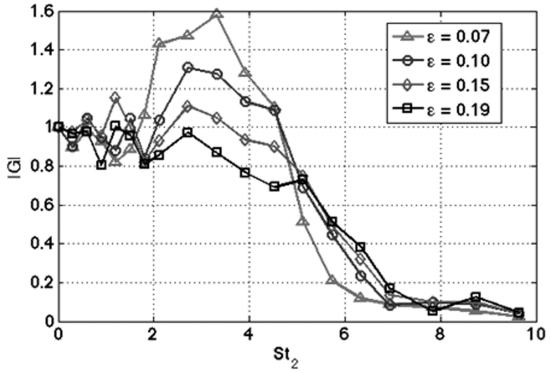

Fig. 20 Experimentally measured gain for an inverted conical flame for a mean velocity $u_o = 2.05$ m/s and $\phi = 0.92$. Data reproduced from Durox et al. [40].

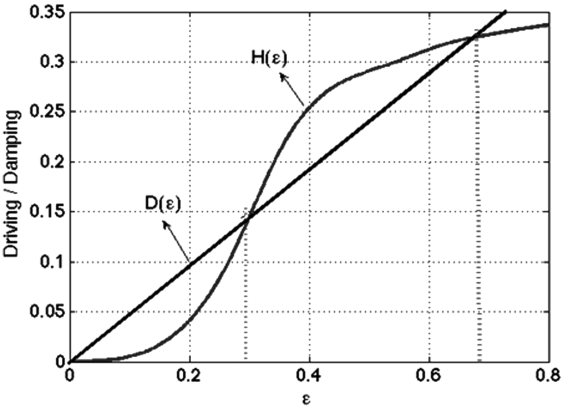

Fig. 22 Dependence of acoustic driving $H(\varepsilon)$ (where $H(\varepsilon)$ is equated for this example to $A'_w/\bar{A}_w$) and damping $D(\varepsilon)$ processes upon velocity amplitude ε for wedge flames at $St_2 = 6.25$ with $K = 2$ and $\alpha = 0.8$.

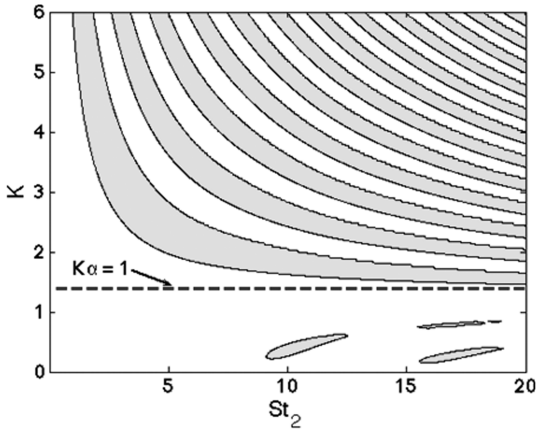

Fig. 23 Qualitative representation of regions in which nonlinear flame transfer exceeds (shaded) or is less than (white) the linear transfer function; $\alpha = 0.8$ and $\varepsilon = 0.1$.

A hypothetical damping curve $D(\varepsilon)$ is also drawn in Fig. 22. Note the 3 intersection points, 2 of which are stable ($\varepsilon = 0$ and $\varepsilon = \varepsilon_{\mathrm{LC}}$) and one of which is unstable ($\varepsilon = \varepsilon_T$). In this case, 2 equally valid solutions are possible, $\varepsilon = 0$ or $\varepsilon = \varepsilon_{\mathrm{LC}}$, and which one the system is actually at depends upon initial conditions. Such a system will manifest characteristics such as hysteresis and triggering (i.e., the destabilization of a linearly stable system by a sufficiently large disturbance [50].

The regions in parameter space (defined by K and St_2) in which the nonlinear transfer function has an inflection point can be determined from the analytical solutions and is shown in Fig. 23. *Note that an inflection point is most likely to exist when the phase speed of the disturbances is less than the mean flow speed* ($K > 1$). This is in accordance with the earlier discussion that showed that nonlinear effects were enhanced for $K > 1$.

We conclude with a few comments on the response of the flame at the first harmonic of the forcing frequency and changes in mean flame characteristics. The previous discussion about the role played by the phase speed of the disturbances, Strouhal number, and the flame aspect ratio upon nonlinearity in flame response is directly applicable here as well, because excitation of harmonics or changes in mean quantities are other manifestations of nonlinearity. These results are not discussed here, but analytical expressions for the flame response at $\omega = 2\omega_o$ are provided in the lead author's thesis [49]. This analysis [49] suggests that the average flame length decreases with increasing Strouhal number (quadratic dependence) and velocity amplitude, trends that are consistent with experiments reported by Durox et al. [24]. Changes in the average flame characteristics (such as its location and length) with increasing disturbance amplitude have been reported in other experimental studies as well [1,8]. These changes have potentially important effects upon the flame-transfer-function phase because they change the time delay between when a disturbance is created and when it encounters the flame.

V. Conclusions

This study has shown that the linear and nonlinear characteristics of the flame dynamics are controlled by the interaction between flame disturbances due to boundaries and flow nonuniformities. A constructive superposition of the two flame disturbance contributions can cause the flame to act as an amplifier at certain frequencies, whereas a destructive superposition can cause the flame response to be identically zero.

In the nonlinear regime, the flame response depends on whether the solution lies in a region of constructive or destructive interference of the flame disturbances. In regions of constructive interference, the nonlinear flame-transfer-function gain is always less than its linear value, whereas in regions of destructive interference, the nonlinear transfer function may exceed its linear value. These characteristics can cause the same combustor to exhibit sub- or supercritical types of bifurcation, depending on the operating condition. The analysis shows that nonlinearity is enhanced and that there is a greater tendency for the nonlinear transfer function to have an inflection point when the phase speed of the disturbances is less than the mean flow speed.

Several additional studies are motivated by this work. First is an analysis of the nonlinear flame response in cases in which the flame is being simultaneously disturbed by deterministic harmonic fluctuations and random fluctuations. The latter fluctuations simulate the impact of background turbulent fluctuations. As such, the analysis would allow for a rudimentary comparison of the nonlinear dynamics of laminar and turbulent flames. Second, the impact of flame-speed modification due to unsteady stretch on the nonlinear response has to be investigated. Linear analysis has shown that the Markstein transfer function for strain, unlike that for curvature, has inverse frequency dependence [51]. A key question then is the relative impact of strain and curvature effects on the flame dynamics at low- and high-velocity amplitudes. In addition, there is a need to couple the flowfield and flame dynamics so that the effect of gas expansion can be captured. This would introduce the temperature jump across the flame as a new parameter into the analysis.

References

[1] Lieuwen, T., and Yang, V. (eds.), *Combustion Instabilities in Gas Turbine Engines*, AIAA, Reston, VA, 2005.

[2] Broda, J. C., Seo, S., Santoro, R. J., Shirhattikar, G., and Yang, V., "An Experimental Study of Combustion Dynamics of a Premixed Swirl Injector," *Proceedings of the Combustion Institute*, Vol. 27, 1998, pp. 1849–1856.

[3] Dowling, A. P., and Stow, S. R., "Acoustic Analysis of Gas Turbine Combustors," *Journal of Propulsion and Power*, Vol. 19, No. 5, 2003, pp. 751–764.

[4] Huang, Y., and Yang, V., "Effect of Swirl on Combustion Dynamics in a Lean Premixed Swirl Stabilized Combustor," *Proceedings of the Combustion Institute*, Vol. 30, No. 2, 2005, pp. 1775–1782. doi:10.1016/j.proci.2004.08.237

[5] Paschereit, C. O., Gutmark, E., and Weisenstein, W., "Control of Thermo-Acoustic Instabilities and Emissions in an Industrial Type Gas Turbine Combustor," *Proceedings of the Combustion Institute*, Vol. 27, 1998, pp. 1817–1824.

[6] Kang, D. M., Culick, F. E. C., and Ratner, A., "Combustion Dynamics of a Low-Swirl Combustor," *Combustion and Flame*, Vol. 151, No. 3, 2007, pp. 412–425. doi:10.1016/j.combustflame.2007.07.017

[7] Dowling, A. P., "Nonlinear Self-Excited Oscillations of a Ducted Flame," *Journal of Fluid Mechanics*, Vol. 346, 1997, pp. 271–290. doi:10.1017/S0022112097006484

[8] Bellows, B., Neumeier, Y., and Lieuwen, T., "Forced Response Studies of a Swirling, Premixed Flame to Flow Disturbances," *Journal of Propulsion and Power*, Vol. 22, No. 5, 2006, pp. 1075–1084. doi:10.2514/1.17426

[9] Lee, J. G., and Santavicca, D. A., "Experimental Diagnostics for the Study of Combustion Instabilities in Lean Premixed Combustors," *Journal of Propulsion and Power*, Vol. 19, No. 5, 2003, pp. 735–750.

[10] Lieuwen, T., and Neumeier, Y., "Nonlinear Pressure-Heat Release Transfer Function Measurements in a Premixed Combustor," *Proceedings of the Combustion Institute*, Vol. 29, No. 1, 2002, pp. 99–105. doi:10.1016/S1540-7489(02)80017-7

[11] Poinsot, T., and Candel, S., "A Nonlinear Model for Ducted Flame Combustion Instabilities," *Combustion Science and Technology*, Vol. 61, Nos. 4–61988, pp. 121–153. doi:10.1080/00102208808915760

[12] Keller, D., and Peters, N., "Transient Pressure Effects in the Evolution Equation for Premixed Flame Fronts," *Theoretical and Computational Fluid Dynamics*, Vol. 6, Nos. 2–3, 1994, pp. 141–159. doi:10.1007/BF00312346

[13] McIntosh, A. C., "Deflagration Fronts and Compressibility," *Philosophical Transactions of the Royal Society of London, Series A: Mathematical and Physical Sciences*, Vol. 357, No. 1764, 1999, pp. 3523–3538. doi:10.1098/rsta.1999.0507

[14] Peters, N., and Ludford, G. S. S., "The Effect of Pressure Variations on Premixed Flames," *Combustion Science and Technology*, Vol. 34,

Nos. 1–61983, pp. 331–344.
doi:10.1080/00102208308923698
[15] Van Harten, A., Kapila, A., and Matkowsky, B. J., "Acoustic Coupling of Flames," *SIAM Journal on Applied Mathematics*, Vol. 44, No. 5, 1984, pp. 982–995.
doi:10.1137/0144069
[16] Peracchio, A. A., and Proscia, W. M., "Nonlinear Heat Release/ Acoustic Model for Thermoacoustic Instability in Lean Premixed Combustors," *Journal of Engineering for Gas Turbines and Power*, Vol. 121, No. 3, 1999, pp. 415–421.
doi:10.1115/1.2818489
[17] Lee, J. G., Kim, K., and Santavicca, D. A., "Measurement of Equivalence Ratio Fluctuation and its Effect on Heat Release during Unstable Combustion," *Proceedings of the Combustion Institute*, Vol. 28, 2000, pp. 415–421.
[18] Dowling, A. P., "A Kinematic Model of a Ducted Flame," *Journal of Fluid Mechanics*, Vol. 394, 1999, pp. 51–72.
doi:10.1017/S0022112099005686
[19] Straub, D. L., and Richards, G. A., "Effect of Fuel Nozzle Configuration on Premix Combustion Dynamics," *American Society of Mechanical Engineers*, American Society of Mechanical Engineers Paper 98-GT-492, 1998.
[20] Baillot, F., Durox, D., and Prud'homme, R., "Experimental and Theoretical Study of a Premixed Vibrating Flame," *Combustion and Flame*, Vol. 88, No. 2, 1992, pp. 149–168.
doi:10.1016/0010-2180(92)90049-U
[21] Lieuwen, T., "Nonlinear Kinematic Response of Premixed Flames to Harmonic Velocity Disturbances," *Proceedings of the Combustion Institute*, Vol. 30, No. 2, 2005, pp. 1725–1732.
doi:10.1016/j.proci.2004.07.020
[22] Shanbhogue, S., Plaks, D., and Lieuwen, T., "The K-H Instability of Reacting, Acoustically Excited Bluff Body Shear Layers," AIAA Paper 2007-5680, 2007.
[23] Bourehla, A., and Baillot, F., "Appearance and Stability of a Laminar Conical Premixed Flame Subjected to an Acoustic Perturbation," *Combustion and Flame*, Vol. 114, Nos. 3–4, 1998, pp. 303–318.
doi:10.1016/S0010-2180(97)00323-4
[24] Durox, D., Baillot, F., Searby, G., and Boyer, L., "On the Shape of Flames under Strong Acoustic Forcing: a Mean Flow Controlled by an Oscillating Flow," *Journal of Fluid Mechanics*, Vol. 350, 1997, pp. 295–310.
doi:10.1017/S0022112097006940
[25] Baillot, F., Bourehla, A., and Durox, D., "The Characteristics Method and Cusped Flame Fronts," *Combustion Science and Technology*, Vol. 112, No. 1, 1996, pp. 327–350.
doi:10.1080/00102209608951963
[26] Blackshear, P. L., "Driving Standing Waves by Heat Addition," *Proceedings of the Combustion Symposium*, Vol. 4, 1953, pp. 553–566.
[27] Ducruix, S., Durox, D., and Candel, S., "Theoretical and Experimental Determinations of the Transfer Function of a Laminar Premixed Flame," *Proceedings of the Combustion Institute*, Vol. 28, 2000, pp. 765–773.
[28] Schuller, T., Durox, D., and Candel, S., "A Unified Model for the Prediction of Laminar Flame Transfer Functions-Comparisons Between Conical and V-Flame Dynamics," *Combustion and Flame*, Vol. 134, Nos. 1–2, 2003, pp. 21–34.
doi:10.1016/S0010-2180(03)00042-7
[29] Fleifel, M., Annaswamy, A. M., Ghoniem, Z. A., and Ghoniem, A. F., "Response of a Laminar Premixed Flame to Flow Oscillations: A Kinematic Model and Thermoacoustic Instability Results," *Combustion and Flame*, Vol. 106, No. 4, 1996, pp. 487–510.
doi:10.1016/0010-2180(96)00049-1
[30] Boyer, L., and Quinard, J., "On the Dynamics of Anchored Flames," *Combustion and Flame*, Vol. 82, No. 1, 1990, pp. 51–65.
doi:10.1016/0010-2180(90)90077-5
[31] You, D. N., Huang, Y., and Yang, V., "A Generalized Model of Acoustic Response of Turbulent Premixed Flame and Its Application to Gas-Turbine Combustion Instability Analysis," *Combustion Science and Technology*, Vol. 177, Nos. 5–6, 2005, pp. 1109–1150.
doi:10.1080/00102200590927012
[32] Lee, D. H., and Lieuwen, T., "Acoustic Near-field Characteristics of a Conical Premixed Flame," *Journal of the Acoustical Society of America*, Vol. 113, No. 1, 2003, pp. 167–177.
doi:10.1121/1.1520547
[33] Searby, G., and Clavin, P., "Weakly Turbulent, Wrinkled Flames in Premixed Gases," *Combustion Science and Technology*, Vol. 46, Nos. 3–6, 1986, pp. 167–193.
doi:10.1080/00102208608959799
[34] Bychkov, V., "Analytical Scalings for Flame Interaction with Sound Waves," *Physics of Fluids*, Vol. 11, No. 10, 1999, pp. 3168–3173.
doi:10.1063/1.870173
[35] Searby, G., and Rochwerger, D., "A Parametric Acoustic Instability in Premixed Flames," *Journal of Fluid Mechanics*, Vol. 231, 1991, pp. 529–543.
doi:10.1017/S002211209100349X
[36] Vaezi, V., and Aldredge, R., "Premixed Flame Propagation in Turbulent Taylor-Couette Flow," *Combustion and Flame*, Vol. 121, Nos. 1–2, 2000, pp. 356–366.
doi:10.1016/S0010-2180(99)00145-5
[37] Hubbard, S., and Dowling, A. P., "Acoustic Instabilities in Premix Burners," AIAA Paper 98-2272, 1998.
[38] Cho, J. H., and Lieuwen, T., "Laminar Premixed Flame Response to Equivalence Ratio Oscillations," *Combustion and Flame*, Vol. 140, No. 1, 2005, pp. 116–129.
doi:10.1016/j.combustflame.2004.10.008
[39] Preetham, Thumuluru, S. K., and Lieuwen, T., "Linear Response of Premixed Flames to Flow Oscillations: Unsteady Stretch Effects," AIAA Paper 2007-0176, 2007.
[40] Durox, D., Schuller, T., and Candel, S., "Combustion Dynamics of Inverted Conical Flames," *Proceedings of the Combustion Institute*, Vol. 30, No. 2, 2005, pp. 1717–1724.
doi:10.1016/j.proci.2004.08.067
[41] Sung, C. J., Sun, C. J., and Law, C. K., "Analytic Description of the Evolution of Two-Dimensional Flame Surfaces," *Combustion and Flame*, Vol. 107, Nos. 1–2, 1996, pp. 114–124.
doi:10.1016/0010-2180(96)00047-8
[42] Michalke, A., "Instability of a Compressible Circular Free Jet with Consideration of the Influence of the Jet Boundary Thickness," NASA TM 75190, 1971.
[43] Bechert, D., and Pfizenmaier, E., "On Wavelike Perturbations in a Free Jet Traveling Faster Than the Mean Flow in the Jet," *Journal of Fluid Mechanics*, Vol. 72, 1975, pp. 341–352.
doi:10.1017/S0022112075003394
[44] Ferguson, D., Richards, G., Woodruff, S., Bernal, S., and Gautam, M., "Effect of Surface Area Variation on Heat Release Rates in Premixed Flames," *Proceedings of the 2nd Joint Meeting of the U. S. Sections of the Combustion Institute*, 2001.
[45] Huang, Y., Sung, H. G., Hsieh, S. Y., and Yang, V., "Large-Eddy Simulation of Combustion Dynamics of Lean-Premixed Swirl-Stabilized Combustor," *Journal of Propulsion and Power*, Vol. 19, No. 5, 2003, pp. 782–794.
[46] Birbaud, A. L., Durox, D., and Candel, S., "Upstream Flow Dynamics of a Laminar Premixed Conical Flame Submitted to Acoustic Modulations," *Combustion and Flame*, Vol. 146, No. 3, 2006, pp. 541–552.
doi:10.1016/j.combustflame.2006.05.001
[47] Jiang, G., and Peng, D., "Weighted ENO Schemes for Hamilton-Jacobi Equations," *SIAM Journal on Scientific Computing*, Vol. 21, No. 6, 2000, pp. 2126–2143.
doi:10.1137/S106482759732455X
[48] Gottlieb, S., and Shu, C., "Total Variation Diminishing Runge-Kutta Schemes," *Mathematics of Computation*, Vol. 67, 1998, pp. 73–85.
doi:10.1090/S0025-5718-98-00913-2
[49] Preetham, "Modeling the Response of Premixed Flames to Flow Disturbances," Ph.D. Thesis, Georgia Inst. of Technology, Atlanta, 2007.
[50] Wicker, J. M., Greene, W. D., Kim, S., and Yang, V., "Triggering of Longitudinal Combustion Instabilities in Rocket Motors—Nonlinear Combustion Response," *Journal of Propulsion and Power*, Vol. 12, No. 6, 1996, pp. 1148–1156.
doi:10.2514/3.24155
[51] Joulin, G., "On the Response of Premixed Flames to Time-Dependent Stretch and Curvature," *Combustion Science and Technology*, Vol. 97, Nos. 1–3, 1994, pp. 219–229.
doi:10.1080/00102209408935375

V. Yang
Editor-in-Chief